RSC Advances

PAPER

View Article Online
View Journal | View Issue

Cite this: *RSC Adv.*, 2020, **10**, 40047

Ce regulated surface properties of Mn/SAPO-34 for improved NH_3-SCR at low temperature†

Qizhi Chen,[ac] Yong Yang,[b] Hang Luo,[b] Zuohua Liu,[b] Zhangfa Tong,[a] Changyuan Tao[b] and Jun Du *[b]

Received 31st July 2020
Accepted 20th October 2020

DOI: 10.1039/d0ra06639g

rsc.li/rsc-advances

Ce modified MnO_x/SAPO-34 was prepared and investigated for low-temperature selective catalytic reduction of NO_x with ammonia (NH_3-SCR). The 0.3Ce–Mn/SAPO-34 catalyst had nearly 95% NO conversion at 200–350 °C at a space velocity of 10 000 h^{-1}. Microporous SAPO-34 as the support provided the catalyst with increased hydrothermal stability. XPS and H_2-TPR results proved that the Mn^{4+} and O_α content increased after incorporation of Ce, this promoted the conversion of NO at low temperature *via* a 'fast SCR' route. NH_3-TPD measurements combined oxidation experiments of NO, NH_3 indicated the reduction of both the surface acidity and the amount of acid sites, which effectively decreased the NH_3 oxditaion to NO or N_2O at elevated temperature and promoted the catalytic selectivity for nitrogen. A redox cycle between manganese oxide and Ce was assumed for the active oxygen transfer and facilitated the catalyst durability.

1 Introduction

Selective catalytic reduction by NH_3 (NH_3-SCR) is known as one of the most efficient ways to remove NO_x from stationary sources.[1] The involved major reaction is

$$4NH_3 + 4NO + O_2 = 4N_2 + 6H_2O \quad (1)$$

The widely used commercial catalysts for NH_3-SCR are V_2O_5–WO_3/TiO_2 and V_2O_5–MoO_3/TiO_2.[2,3] As the catalyst works at a relative high temperature of 300–400 °C, it is usually located upstream of both the desulfurizer and the electrostatic precipitator, which causes the toxicity of vanadium species by sulfur and dust in the flue gas.[4,5] Therefore, it is of great significance to develop low-temperature NH_3-SCR catalysts so that the SCR reactor can be placed downstream of the desulfurizer and electrostatic precipitator to significantly improve the economics of NH_3-SCR.

Transition metal including Fe, Mn, Cu and Ni supported on different commercial carriers have been investigated for the low-temperature NH_3-SCR.[6–8] Manganese based catalysts show good performances of low-temperature catalytic activity, for manganese oxides containing various types of labile oxygen and different oxidation states of Mn (Mn^{2+}, Mn^{3+}, and Mn^{4+}), which are necessary to complete a catalytic cycle.[9–12] But the selectivity for nitrogen was limited at elevated temperature, for the obvious oxidation of ammonia on manganese oxide surface, especially on the highly crystalline surface. Therefore, the remediation of redox properties of manganese oxide would be a viable route for inhibiting the ammonia oxidation. The doped manganese oxide has been investigated for NH_3-SCR catalyst.[13] As an inexpensive and a relatively nontoxic material, Ce has also been widely used as doping agent for its excellent redox properties and the great oxygen storages associated with plenty of oxygen vacancies.[14–16] Ce modified Fe-ZSM-5 catalyst showed an improved NH_3-SCR activity, which was ascribed to the enhanced oxidation of NO to NO_2.[17] Yang and Qi carried out systematically studies on Ce–Mn mixed oxide catalyst without supports. The results yielded nearly 100% conversion for NO at 120 °C at a high space velocity of 42 000 h^{-1}, but N_2O was observed as the temperature higher than 150 °C, indicated the complexity of the oxidation mechanism.[18]

Compared with the pure manganese oxide, supported one will provide highly spreading manganese oxide and would decrease the crystalline which are benefited for increase catalytic selectivity.[19–23] So combined with the consideration of mechanical strength for engineering allocation, the conventional supported manganese oxide had been widely applied for this low-temperature SCR catalyst.[20] It was reported that the molecular sieves (ZSM, beta) show high activities in NH_3-SCR when used in supported Cu catalyst, but suffer from narrow activity window and hydrothermal deteriorations, which restrict its further commercial applications for NH_3-SCR.[24,25] As a chabazite type microporous molecular sieve with CHA structure, SAPO-34 can not only significantly improve the activity and

[a]*School of Chemistry and Chemical Engineering, Guangxi University, Nanning 530004, China*

[b]*College of Chemistry and Chemical Engineering, Chongqing University, Chongqing 401331, China. E-mail: dujune@cqu.edu.cn*

[c]*Guangxi Huiyuan Manganese Industry Co., Ltd., China*

† Electronic supplementary information (ESI) available. See DOI: 10.1039/d0ra06639g

selectivity of the composite catalyst,[26,27] but also has excellent hydrothermal stability and resistance to SO_2 poisoning, thereby prolonging the service life of the catalyst in the high-activity zone.[28,29] Much of significant contributions had been made for Cu-based zeolite catalyst.[30] The previous researches revealed the exact location of active sites and confirmed the isolated Cu^{2+} ions as active sites over Cu/SSZ-13 catalysts and Cu/CHA catalyst.[31,32] Furthermore, Li Wei and co-work clarified the isolated Cu^{2+} ion located on the plane of the six-membered ring of SAPO-34, which appeared to be responsible for the excellent SCR activity and N_2 selectivity.[33] Based on the previous reorganization of Cu–zeolite based SCR catalysts, the position of the active species on molecular sieves reflected the interaction of active species with zeolite supports, and finally composed the surface acidity and redox cycle exist along with NH_3-SCR route. Therefore, correlation the surface redoxity and acidity cycle of active species with the NH_3-SCR activity and selectivity would provide a directly understanding for the zeolite-based SCR catalyst.

Therein, based on microporous zeolite materials as support and manganese oxides as active species aimed to the low temperature NH_3-SCR process, we prepared the SCR catalyst of Ce modified manganese oxides supported on SAPO-34 zeolite. The as-prepared catalysts were characterized and the effects of Ce on the surface property such as redoxity and acidity of the Mn/SAPO-34 catalyst were analysed. The catalytic performances of Ce modified Mn/SAPO-34 catalyst as well as the hydrothermal stability of the catalyst were evaluated. The surface acidity and redox cycles of Ce modified Mn/SAPO-34 catalyst was discussed and correlated with NH_3-SCR performances.

2 Experimental section

2.1 Catalyst preparation

The synthesis of SAPO-34 molecular sieve: with phosphoric acid, pseudo boehmite, tetraethyl orthosilicate and morpholine as sources, a gel with the molar ratio of 1.0 Al_2O_3 : 1.1 P_2O_5 : 0.6 SiO_2 : 2.1 morpholine : 66.0 H_2O was prepared. After aging at room temperature for 12 hours, the temperature was increased to 200 °C at a heating rate of 3°C min^{-1} and kept at this temperature for 48 hours to crystallize. The obtained solid crystallized product was washed with deionized water to neutrality, dried and then calcined at 550 °C for 5 hours to obtain SAPO-34 molecular sieve. The synthesis of Mn/SAPO-34 or *x*Ce–Mn/SAPO-34: the ultrasonic impregnation method was used to synthesized the Mn/SAPO-34 or *x*Ce–Mn/SAPO-34. Typically, a certain amount of acetylacetone manganese(II) salt dehydrator, or cerium nitrate mixed with acetylacetone manganese(II) salt dehydrate (only changed the Ce/Mn ratio and kept the total amount of Ce ($Ce(NO)_3 \cdot 6H_2O$) and Mn ($Mn(CH_3COO)_2$) precursors consistent (0.8922 g) for all samples) was dissolved in acetone (60 mL) at room temperature. Then the SAPO-34 powder (3.0 g) was added into the above solution with 1 h ultrasonic treatment to obtain catalyst precursors after evaporating the solvent, followed by calcined at 400 °C in air for 5 hs. The resulted catalysts were designated as Mn/SAPO-34 or *x*Ce–Mn/SAPO-34, where *x* represented the mole ratio of the Ce/Mn, specifically from 0.1 to 0.4.

2.2 Catalytic activity measurements

The NH_3-SCR activity was measured in a continuous flow fixed-bed stainless steel reactor using 1.57 mL 40–60 mesh catalyst at atmospheric pressure. The simulated flue gases consisted of 500 ppm NO, 500 ppm NH_3, 5 vol% O_2, and balanced with N_2. The gas hourly space velocity (GHSV) was 10 000 h^{-1}. The concentrations of NO, NO_2, N_2O and NH_3 were determined using a flue gas analyser (Sensonic 4000, Sensonic). The reaction temperature was scheduled from 100 °C to 450 °C. The NO conversion (η_{NO}) and N_2 selectivity were calculated by measuring the concentration of effluent gases according to the following equations:

$$\eta_{NO} = \frac{[NO]_{in} - [NO]_{out}}{[NO]_{in}} \times 100\% \quad (2)$$

$$N_2 \text{ selectivity} = \frac{[NO]_{in} - [NO]_{out} + [NH_3]_{in} - [NH_3]_{out} + [NO]_{out} - 2[N_2O]_{out}}{[NO]_{in} - [NO]_{out} + [NH_3]_{in} - [NH_3]_{out}} \times 100\% \quad (3)$$

2.3 Characterization of catalyst

The specific surface areas of the catalysts were measured by nitrogen adsorption and desorption method on 3H-2000PS1 (BeiShiDe instrument, China), using the Brunauer–Emmett–Teller (BET) model. The scanning electron microscopy (SEM) images were obtained using a field-emission scanning electron microscopy (JSM-7800F, JEOL, Japan), at the operation voltage of 5 kV. The X-ray diffraction (XRD) patterns of the samples were obtained with a Rigaku D/max-3C diffract meter with Cu Kα radiation ($\lambda = 1.54056$ Å) operating at 40 kV and 30 mA. The XRD patterns were collected in the 2θ range of 5–90° with a scanning step size of 0.02° and scanning rate of 10° min^{-1}. The X-ray photoelectron spectroscopy (XPS) was performed on a PHI quant era II (Ulvac-Phi, Japan) under an ultra-high vacuum, using a monochromated Al Kα source (1486.6 eV) at 42.1 W. The measurements were performed at 20 eV pass energy, 0.1 eV step and 0.15 dwelling time. All the binding energies were corrected with reference to the C 1s peak at 284.8 eV.

The temperature programmed reduction with hydrogen (H_2-TPR) were conducted on an automatic multifunction adsorption instrument (TP-5080, China) with 50 mg sample, the test ranged from 30 °C to 700 °C at a heating rate of 10 °C min^{-1} with a reducing gas consist of 10 vol% H_2 and 90% N_2 at the 30 mL min^{-1} flow rate. The NH_3-temperature programmed desorption (NH_3-TPD) measurements were carried out under the similar conditions with 100 mg sample after purged with He at 300 °C for half an hour. The inlet gas consisted of 5 vol% NH_3 balanced with helium.

3 Results and discussion

3.1 NH_3-SCR performances

The Ce modified Mn/SAPO-34 catalysts exhibited a superior catalytic activity, with the NO conversion exceeding 80% in the range of

200–350 °C, achieved the best performance at 300 °C. The addition of cerium obviously expanded the temperature windows towards the lower temperature range, accompanying with the improved NO conversion (>90%) at 200–350 °C. The active temperature window of the Ce modified catalyst was wider about 100 °C than the unmodified sample, whose diminished temperature windows was 250–300 °C and NO conversion below 85%.

The N_2 selectivity of the catalysts was displayed in Fig. 1b. The Ce–Mn/SAPO-34 catalysts with different Ce/Mn ratios showed an increased N_2 selectivity as cerium introduced, and the best performance of the catalysts for N_2 selectivity (over 90% from 100–400 °C) was achieved at the Ce/Mn molar ratio of 0.3, illustrating that the presence of Ce enhanced the main reaction with the product of N_2.

3.2 Hydrothermal stability of catalysts

The catalyst resistance to H_2O is one of the important indicators for the SCR catalyst. The hydrothermal stability of Mn/SAPO-34 and Ce–Mn/SAPO-34 catalysts were further studied by performing steaming treatments at 700 °C for 12 hours in flowing gas containing 10 vol% H_2O and 90% air. The catalytic performances of the as-aged catalyst were presented in Fig. 2. It can be seen that the aged Mn/SAPO-34 catalyst showed poor activity, especially at low-temperatures (*i.e.*, 150–200 °C); whereas the aged Ce modified Mn/SAPO-34 catalysts could maintain activity at low-temperatures range and show some declined NO conversion at the elevated temperature range. Among those, the aged 0.3Ce–Mn/SAPO-34 catalyst exhibited the optimal catalytic performance with the maximum value of NO conversion nearly 80% in the range of 200–300 °C.

3.3 Morphology and physical properties of the catalyst

3.3.1 Texture analysis. The texture structures of the Mn/SAPO-34 and Ce–Mn/SAPO-34catalysts were investigated by BET (Fig. S1a†). Type I isotherm curves for the catalysts were observed, typical for a microporous solid. The pores of the Mn/SAPO-34 and Ce–Mn/SAPO-34 catalysts are mostly distributed in the range of 3.3–3.7 nm (Fig. S1b†). Based on the BET specific surface area and pore volume of the Mn/SAPO-34 and Ce–Mn/SAPO-34 catalysts (Table S1†), it could be concluded that the modification of Ce significantly reduces the BET surface area, pore volume and pore diameter of the catalyst. For Mn/SAPO-34, the BET surface area and pore diameter were 416.57 $m^2\ g^{-1}$ and 3.66 nm, as *n*(Ce/Mn) in Ce–Mn/SAPO-34 catalysts increased from 0.1 to 0.4, the BET surface area and pore diameter were decreased to 370.07 $m^2\ g^{-1}$ and 3.32 nm, respectively, indicating that the part of the cerium oxide entered into the interior of the SAPO-34 molecular sieve carrier in addition to loading on the surface.

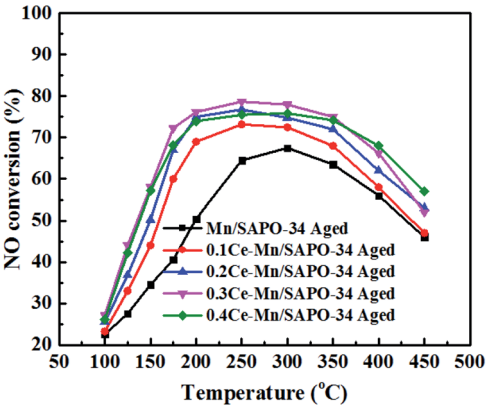

Fig. 2 Catalytic performances of hydrothermally aged catalysts in the NH_3-SCR process. (Hydrothermal aging conditions: 10 vol% H_2O and 90% air, total flow rate = 200 mL min^{-1}, aging time = 12 hours, aging temperature = 700 °C. The reaction condition: [NH_3] = [NO] = 500 ppm, [O_2] = 5 vol%, N_2 balance and GHSV = 10 000 h^{-1}).

The aged catalyst showed declined BET area and pore volumes. For aged 0.3Ce–Mn/SAPO-34 catalysts, the BET areas and pore volume decreased from 375.75 to 359.21 $m^2\ g^{-1}$, and 0.169 to 0.0514 $cm^3\ g^{-1}$ respectively (Fig. S2 and Table S2†). The observed decreased NO conversion over the aged-catalyst would be ascribed in certain degree to the diminish of BET area and pore volume.

3.3.2 SEM and XRD analysis. The SEM image (Fig. 3) depicts the surface morphology of the Mn/SAPO-34 and Ce–Mn/SAPO-34 catalysts, with a crystal size of about 3 μm and with

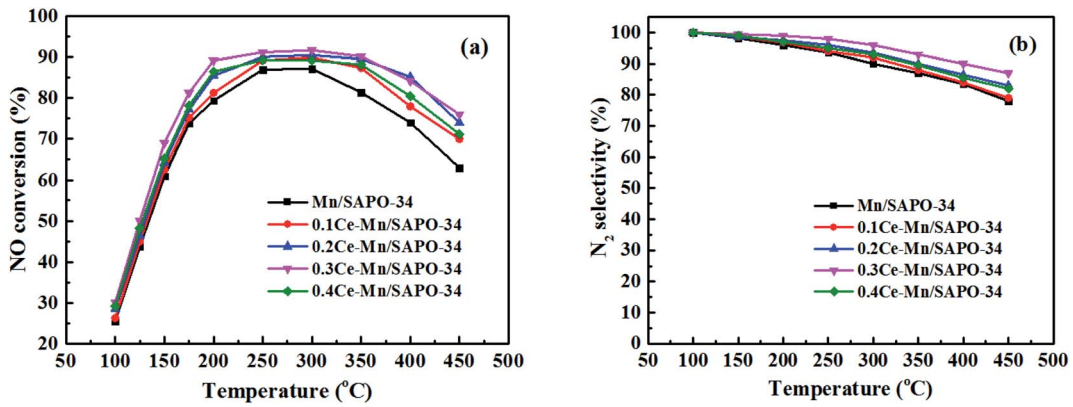

Fig. 1 Catalytic performances of Mn/SAPO-34 and Ce–Mn/SAPO-34: (a) NO conversion, (b) the N_2 selectivity in the NH_3-SCR reaction. (The reaction condition: [NH_3] = [NO] = 500 ppm, [O_2] = 5 vol%, N_2 balance and GHSV = 10 000 h^{-1}).

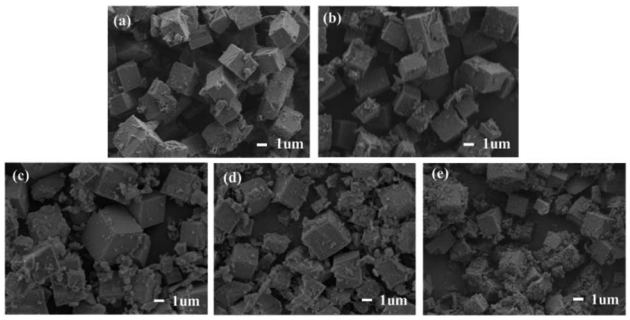

Fig. 3 The SEM images of Mn/SAPO-34 and Ce–Mn/SAPO-34 catalysts: (a) Mn/SAPO-34, (b) 0.1Ce–Mn/SAPO-34, (c) 0.2Ce–Mn/SAPO-34, (d) 0.3Ce–Mn/SAPO-34, (e) 0.4Ce–Mn/SAPO-34.

a typical cubic structure of CHA,[34] which is consistent with the following XRD results. The Mn/SAPO-34 catalyst exhibits a smooth surface, and there are some small particles between the cubic or on the surface. For the Ce modified catalysts, the surface is covered with randomly shaped material. As Ce content increased, the crystallinity of the Ce–Mn/SAPO-34 catalysts reduced significantly, this was consisted with XRD results (Fig. 4).

For Mn/SAPO-34 and Ce–Mn/SAPO-34 catalyst, both have diffraction peaks of the chabazite phase, an indication of typical CHA structures (Fig. 4). In addition, no diffraction peaks associated with cerium oxides or manganese oxides were observed. This indicates that the Ce or Mn were predominantly present in amorphous combined with the SEM results. As compared with the Mn/SAPO-34 catalyst, the intensities of the main diffraction peak of Ce–Mn/SAPO-34 catalysts gradually diminished by increasing the Ce content, implying the modification of Ce reduced the crystallinity of Mn/SAPO-34 catalyst. In particular, the XRD pattern of the 0.4Ce–Mn/SAPO-34 catalyst with the largest Ce loading amount where the intensity of the reflection with maximum is much lower than the one in Mn/SAPO-34 catalyst.

3.3.3 NH_3-TPD of the catalyst. The surface acidity of the catalysts was obtained based on NH_3-TPD measurement (Fig. 5, Table S3†). The two NH_3 desorption peaks were observed over a wide temperature range due to the variability of the adsorbed

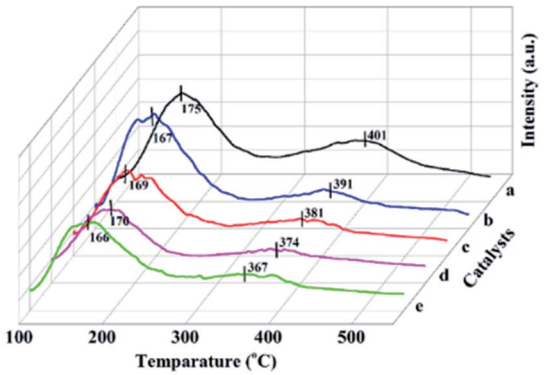

Fig. 5 NH_3-TPD profiles of Mn/SAPO-34 and Ce–Mn/SAPO-34 catalysts. (a) Mn/SAPO-34, (b) 0.1Ce–Mn/SAPO-34, (c) 0.2Ce–Mn/SAPO-34, (d) 0.3Ce–Mn/SAPO-34, (e) 0.4Ce–Mn/SAPO-34.

NH_3 species with different thermal stabilities. The desorption peak around 170 °C, can be attributed to physical or weakly adsorbed NH_3. The peak between 380 °C and 405 °C, can be attributed to stronger acid sites generated by the incorporation of silicon atoms into the framework of SAPO-34 molecular sieves during the formation process. After Ce doping, the weak acid sites of the catalysts showed little change, but the peaks related to the NH_3 desorbing from strong acid sites were observed shifting to lower temperature, namely, from *c.a.* 400 °C on Mn/SAPO-34 to 374 °C over 0.3Ce–Mn/SAPO-34, accompanying with the weakening of the peak. This indicates the weak acidity and reduced amount of acid sites, which was responsible for the suppressed NH_3 oxidation reaction and inverse the enhanced catalytic selectivity for nitrogen.

3.3.4 H_2-TPR analysis. The redox ability over the catalysts containing Mn and Ce species is considered a key factor for the catalytic cycle of NH_3-SCR reaction.[35] which was demonstrated *via* H_2-TPR measurement (Fig. 6). Three reduction peaks were observed in the range of 300–700 °C for the Mn/SAPO-34 catalyst, the low-temperature reduction peak at 384 °C could correlate to the reduction of MnO_2 to Mn_2O_3, and the reduction peak near 494 °C, corresponding to the reduction of Mn_2O_3 to Mn_3O_4. Meanwhile, the high-temperature reduction peak at

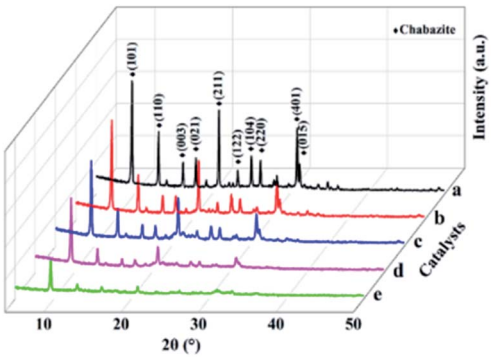

Fig. 4 The XRD patterns of Mn/SAPO-34 and Ce–Mn/SAPO-34 catalysts. (a) Mn/SAPO-34, (b) 0.1Ce–Mn/SAPO-34, (c) 0.2Ce–Mn/SAPO-34, (d) 0.3Ce–Mn/SAPO-34, (e) 0.4Ce–Mn/SAPO-34.

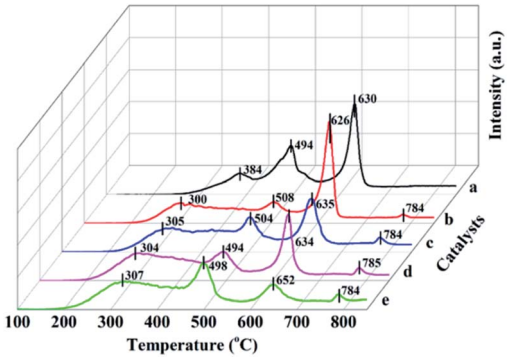

Fig. 6 H_2-TPR profiles of Mn/SAPO-34 and Ce–Mn/SAPO-34 catalysts. (a) Mn/SAPO-34, (b) 0.1Ce–Mn/SAPO-34, (c) 0.2Ce–Mn/SAPO-34, (d) 0.3Ce–Mn/SAPO-34, (e) 0.4Ce–Mn/SAPO-34.

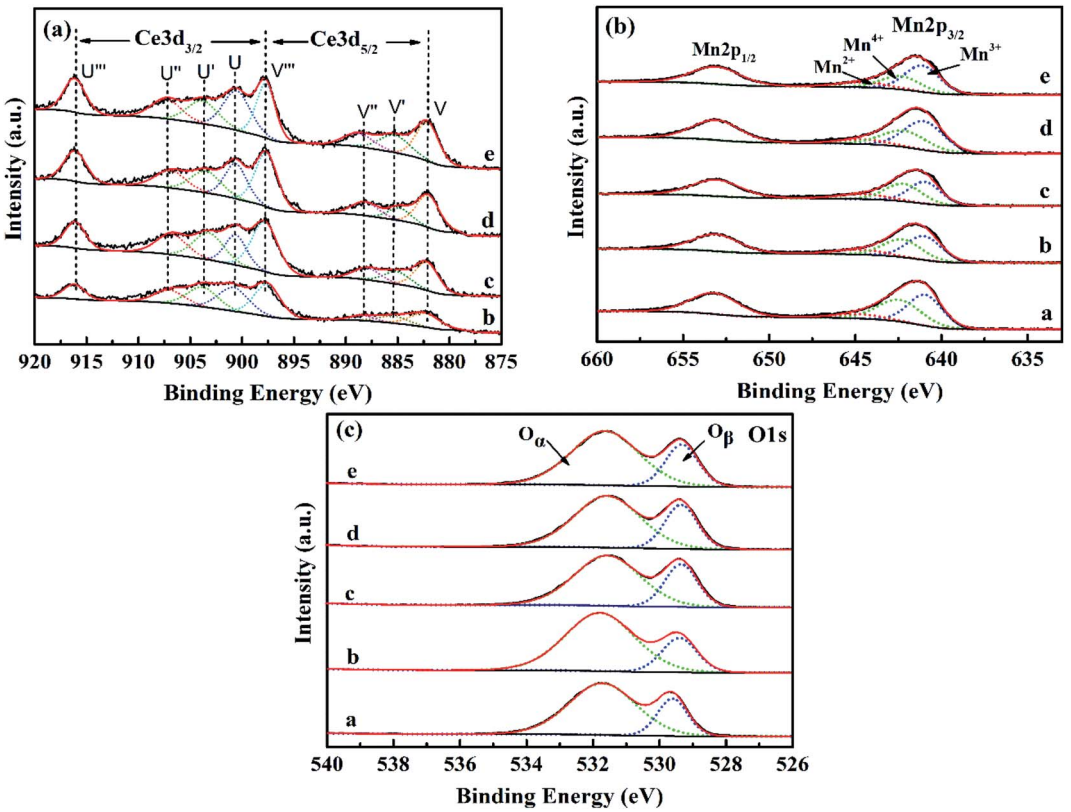

Fig. 7 (a) Mn 2p, (b) Ce 3d and (c) O 1s XPS spectra of Mn/SAPO-34 and Ce–Mn/SAPO-34 catalysts. a: Mn/SAPO-34, b: 0.1Ce–Mn/SAPO-34, c: 0.2Ce–Mn/SAPO-34, d: 0.3Ce–Mn/SAPO-34, e: 0.4Ce–Mn/SAPO-34.

630 °C was interpreted as a reduction of Mn_3O_4 to MnO.[36] The following equation depicted the reduction process of MnO_x in Mn/SAPO-34 catalyst.[37]

$$MnO_2 \rightarrow Mn_2O_3 \rightarrow Mn_3O_4 \rightarrow MnO \quad (4)$$

For the Ce modified catalysts a broad peak is observed around 300 °C, which show much broader than that of Mn/SAPO-34 catalyst. The initial temperature of the peak over the Ce modified catalyst shifted to lower temperature, from 384 °C to 300 °C. This indicates the introduction of Ce not only alters the surface acidities, but also enhances the redox activity at low-temperature *via* the interaction between Mn and Ce species. This would be responsible for the increased low-temperature catalytic activity over Ce modified catalyst.

3.3.5 XPS analysis. The surface chemical composition and oxidation states of these synthesized catalysts were further investigated by XPS. High resolution spectra from Ce 3d, Mn 2p, and O 1 s are displayed in Fig. 7. For the Ce 3d spectrum (Fig. 7a), all samples exhibited eight characteristic peaks in the range of 920–875 eV, and are labelled as u‴, u″, u′, u, v‴, v″, v′, and v. The u′ and v′ peaks can be attributed to Ce^{3+} species, while the u‴, u″, u, v‴, v″, and v peaks can be assigned to Ce^{4+} species.[38] From these peaks, we can learn that the Ce^{4+} oxidation state is predominant.

For the Mn 2p spectrum (Fig. 7b), two main peaks (643 eV and 654 eV) are apparently attributed to Mn $2p_{3/2}$ and Mn $2p_{1/2}$. By performing peak-fitting deconvolutions, the Mn $2p_{3/2}$ peaks can be divided into three characteristic peaks, which are assigned to Mn^{3+} (640.4 eV), Mn^{4+} (642.2 eV) and Mn^{2+} (644.5 eV), respectively. Previous studies have shown that Mn^{4+} species have favourable redox properties for NO conversion.[16] Therefore, the relative content of surface Mn^{4+} ($Mn^{4+}/(Mn^{2+} + Mn^{3+} + Mn^{4+})$) and Ce^{3+}($Ce^{3+}/(Ce^{3+} + Ce^{4+})$) of these Ce–Mn/SAPO-34 catalysts were calculated, and listed in Table 1. The surface Mn^{4+} content of the 0.3Ce–Mn/SAPO-34 catalyst was higher than that over Mn/SAPO-34 catalyst. More specifically, at low loadings, the activity and selectivity increased with the increase of Ce loading (*c.a.* the atomic ratio of Ce/Mn gradually increase), and the best catalytic performance appeared at the Ce/Mn ratio of 49.05%, it gave 90.3% NO conversion and 98.5% selectivity for N_2. However, the activity and selectivity would decrease significantly when the Ce/Mn ratio is higher than 49.05%. It furtherly confirmed that this catalytic system showed synergic effect between Ce and Mn and this subsequently improved the activity and selectivity of NH_3-SCR. (Table S4†) This was attributed to the electronic interactions between manganese oxide and Ce, which consequently resulted in the redox equilibrium of $Mn^{3+} + Ce^{4+} \leftrightarrow Mn^{4+} + Ce^{3+}$ shifting to the Mn^{4+} formation.

The O 1 s spectrum (Fig. 7c) of these synthesized catalysts, which exhibited a strong peak at 529.1 eV, and a shoulder at a higher binding energy of 531.2 eV, attributable to lattice oxygen (labelled as O_β) and adsorbed oxygen (labelled as O_α) on

Table 1 The surface composition and states of the catalysts from XPS analysis

	Atomic concentration (%)				Atomic ratio (%)		
Samples	Ce	Mn	O	Ce/Mn	$Ce^{3+}/(Ce^{3+} + Ce^{4+})$	$Mn^{4+}/(Mn^{2+} + Mn^{3+} + Mn^{4+})$	$O_\alpha/(O_\alpha + O_\beta)$
Mn/SAPO-34	0	18.24	47.88	0.00	0	46.22	71.84
0.1Ce–Mn/SAPO-34	1.52	16.31	45.63	9.32	11.54	48.35	74.38
0.2Ce–Mn/SAPO-34	4.19	15.35	43.35	27.30	12.32	47.61	75.65
0.3Ce–Mn/SAPO-34	6.95	14.17	42.58	49.05	13.92	51.27	76.98
0.4Ce–Mn/SAPO-34	9.24	12.63	40.65	73.16	13.28	43.58	76.36

the surface of these samples, respectively.[39] It has been widely reported that oxygen in the gas phase can be activated by oxygen vacancies on the surface of deNO catalysts to form surface adsorbed oxygen. This effect may also enhance catalytic performance in the NH_3-SCR reaction.[40] Furthermore, a process of oxygen storage/release betweenCe^{3+} and Ce^{4+} has been proposed in the following equations: (a) $2CeO_2 \rightarrow Ce_2O_3 + O^*$ (adsorbed oxygen) and (b) $Ce_2O_3 + 1/2O_2 \rightarrow 2CeO_2$. The increased O_α content can promote the oxidation of NO to NO_2 and enhance the catalytic performance of the low-temperature deNO catalysts through a "fast NH_3-SCR" route.

3.4 Redox performances of Ce–Mn/SAPO-34 catalyst

The oxidation of NH_3 to NO_x was examed (Fig. 8). Here, N_2O and NO generated in the NH_3 oxidation reaction were detected as temperature higher than 250 °C, and the amount of N_2O and NO increased with the temperature. Compared with the Mn/SAPO-34 catalyst, the Ce–Mn/SAPO-34 catalyst exhibits lower N_2O and NO concentration in the NH_3 oxidation product. The results indicated the NH_3 oxidation was suppressed on Ce modified catalyst at elevated temperature, by reducing acid amount and weak acidity on surface as expressed by NH_3-TPD measurement, leading to the improved catalytic selectivity performance of NH_3-SCR.

With Ce modified Mn/SAPO-34 catalyst, the NO oxidation activity increased significantly (Fig. 9), which suggested that the addition of Ce can increase the oxidation rate of NO to NO_2. This was ascribed to the excellent redox properties associated with the existence of the Ce^{4+}/Ce^{3+} redox couple and high oxygen storage/release capacity, which corresponding to the oxygen vacancies at interface between metal oxides. Therefore, the higher NO conversion was observed *via* promoted NO oxidation to NO_2 at low-temperature, resulted from the 'fast NH_3-SCR' route.[28,29]

Therefore, the introducing of Ce regulated the following cycle by inducing the formation of Mn^{4+} at low temperature and reducing the acidity and the amount of acid sites on surface of

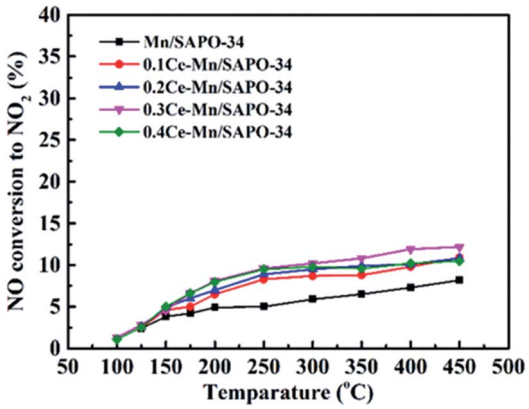

Fig. 9 NO oxidation to NO_2 experiment. (The reactant condition: [NO] = 500 ppm, $[O_2]$ = 5 vol%, N_2 balance and GHSV = 10 000 h^{-1}).

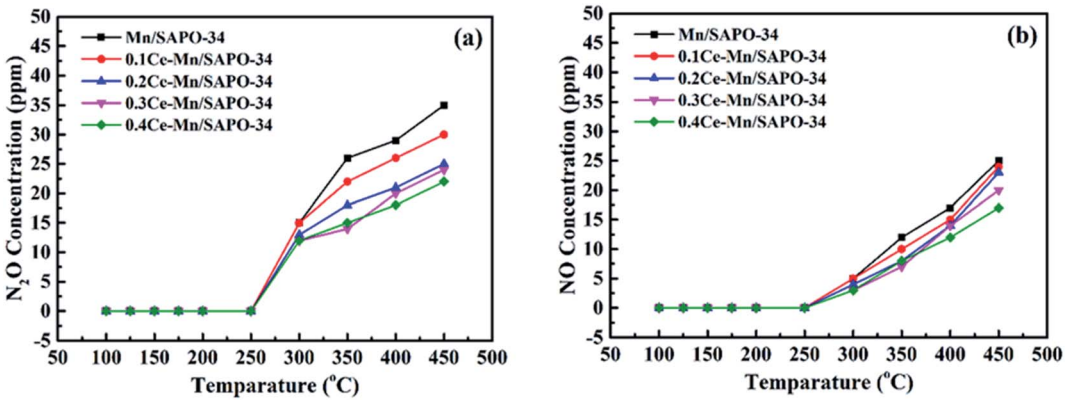

Fig. 8 The concentration of N_2O (a) and NO (b) generated in the NH_3 oxidation. (The reactant condition: $[NH_3]$ = 500 ppm, $[O_2]$ = 5 vol%, N_2 balance and GHSV = 10 000 h^{-1}).

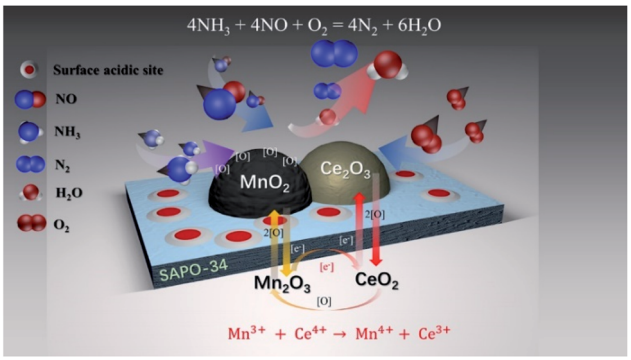

Scheme 1 The catalytic mechanism schematic diagram for Ce–Mn/SAPO-34 in 'NH_3-SCR' process.

Ce–Mn/SAPO-34 catalyst (Scheme 1), following $Mn^{3+} + Ce^{4+} \rightarrow Mn^{4+} + Ce^{4+}$. The enriched Mn^{4+} facilitated the NO oxidation to NO_2, and improved the conversion of NO at low-temperatures following a fast NH_3-SCR'route. Subsequently, the partially reduced Ce was oxidized to Ce^{4+} accompanying with the generation of active oxygen species. The weak acidity and reduced acid amount suppressed the reaction of NH_3 oxidation to N_2O or NO, which would improve the selectivity for nitrogen at elevated temperature.

4 Conclusions

In summary, Ce modified MnO_x/SAPO-34 catalysts were prepared and evaluated for low-temperature NH_3-SCR. The as-prepared catalysts showed high activity and selectivity for NO reduction with NH_3 at low-temperature. Above 90% NO conversion was obtained on 0.3Ce–Mn/SAPO-34 catalyst at 200 °C with a GHSV of 10 000 h^{-1}. Ce could substantially enhance the redox activity of Mn/SAPO-34 by formatting Mn^{4+} at low-temperature, resulting from the electronic interaction between manganese oxide and Ce. The redox cycle between manganese oxides and Ce of different valences accompanied with the generation and transition of active oxygen species. Subsequently, the introducing of Ce can improve the NO oxidation to NO_2 and increase the conversion of NO at low-temperatures following a "fast NH_3-SCR" route. Ce regulated Mn/SAPO-34 catalyst with weak acidity and reduced acid amount on surface were observed, which significantly suppressed the oxidation of NH_3 at the elevated temperature, and facilitated the increase of catalytic selectivity.

Conflicts of interest

There are no conflicts to declare.

Acknowledgements

The authors would like to thank the financial support by Innovation and Development Project of Guangxi Science and Technology Department (Project Grants 809274011004).

References

1 G. Busca, L. Lietti, G. Ramis and F. Berti, *Appl. Catal., B*, 1998, **18**, 1.
2 C. Ciardelli, I. Nova, E. Tronconi, D. Chatterjee, B. Bandl-Konrad, M. Weibel and B. Krutzsch, *Appl. Catal., B*, 2007, **70**, 80.
3 I. Nova, C. Ciardelli, E. Tronconi, D. Chatterjee and B. Bandl-Konrad, *Catal. Today*, 2006, **114**, 3.
4 J. Li, H. Chang, L. Ma, J. Hao and R. Yang, *Catal. Today*, 2011, **175**, 147.
5 W. S. Kijlstra, M. Biervliet, E. K. Poels and A. Bliek, *Appl. Catal., B*, 1998, **16**, 327.
6 Z. Qu, L. Miao, H. Wang and Q. Fu, *Chem. Commun.*, 2015, **51**, 956.
7 C. Fang, D. Zhang, S. Cai and L. Zhang, *Nanoscale*, 2013, **5**, 9199.
8 Y. Wan, W. Zhao, Y. Tang and L. Li, *Appl. Catal., B*, 2014, **148**, 114.
9 B. Jiang, Y. Liu and Z. Wu, *J. Hazard. Mater.*, 2009, **162**, 1249.
10 W. S. Kijlstra, D. S. Brands and H. I. Smit. *Preprints-American Chemical Society*. Division of Petroleum Chemistry, 1997.
11 X. Lou, P. Liu and J. Li, *Appl. Surf. Sci.*, 2014, **307**, 382.
12 Z. Wu, B. Jiang and Y. Liu, *J. Hazard. Mater.*, 2007, **145**, 488.
13 Y. Xiong, C. Tang and X. Yao, *Appl. Catal., A*, 2015, **495**, 206.
14 X. Yao, Y. Xiong and W. Zou, *Appl. Catal., B*, 2014, **144**, 152.
15 Z. Liu, Y. Liu and B. Chen, *Catal. Sci. Technol.*, 2016, **6**, 6688–6696.
16 D. Zhang, L. Zhang and L. Shi, *Nanoscale*, 2013, **5**, 1127.
17 G. Carja, G. Delahay and C. Signorile, *Chem. Commun.*, 2004, **35**, 1404.
18 G. Qi and R. T. Yang, *J. Catal.*, 2003, **217**, 434.
19 J. Lia, J. Guoa and X. Shi, *Appl. Surf. Sci.*, 2020, **534**, 147592.
20 P. G. Smirniotis, P. M. Sreekanth and D. A. Pena, *Ind. Eng. Chem. Res.*, 2006, **45**, 6436.
21 F. Cao, J. Xiang and S. Su, *Fuel Process. Technol.*, 2015, **135**, 66–72.
22 S. Ren, S. Li, Z. Su and J. Yang, *Chem. Eng. J.*, 2018, **351**, 540–547.
23 M. Chen, Q. Sun and X. Yang, *Inorg. Chem. Commun.*, 2019, **105**, 203–207.
24 J. H. Kwak, R. G. Tonkyn and D. H. Kim, *J. Catal.*, 2010, **275**, 187.
25 D. W. Fickel, E. D. Addio and J. A. Lauterbach, *Appl. Catal., B*, 2011, **102**, 441–448.
26 R. Zhang, N. Liu and Z. Lei, *Chem. Rev.*, 2016, **116**, 3658.
27 H. I. Hamoud, V. Valtchev and M. Daturi, *Appl. Catal., B*, 2019, **250**, 419–428.
28 A. M. Prakash and S. Unnikrishnan, *J. Chem. Soc., Faraday Trans.*, 1994, **90**, 2291–2296.
29 P. Zhai, Z. M. Li, H. J. Liu and I. L. Li, *Carbon*, 2006, **44**, 1151–1157.
30 S. Mohan, P. Dinesha and S. Kumar, *Chem. Eng. J.*, 2020, **384**, 123253.
31 S. T. Korhonen, D. W. Fickel and R. F. Lobo, *Chem. Commun.*, 2011, **47**, 800.

32 U. Deka, A. Juhin and E. A. Eilertsen, *J. Phys. Chem. C*, 2012, **116**, 4809.
33 J. Xue, X. Wang and G. Qi, *J. Catal.*, 2013, **297**, 56.
34 L. Xu, A. Du and Y. Wei, *Microporous Mesoporous Mater.*, 2008, **115**, 332.
35 S. Wu, X. Yao and L. Zhang, *Chem. Commun.*, 2015, **51**, 3470.
36 L. Wang, B. Huang and Y. Su, *Chem. Eng. J.*, 2012, **192**, 232.
37 F. Kapteijn, L. Singoredjo and A. Andreini, *Appl. Catal., B*, 1994, **3**, 173.
38 M. Romeo, K. Bak and J. Elfallah, *Surf. Interface Anal.*, 1993, **20**, 508.
39 G. Carja, Y. Kameshima and K. Okada, *Appl. Catal., B*, 2007, **73**, 60.
40 P. R. Ettireddy, N. Ettireddy and T. Boningari, *J. Catal.*, 2012, **292**, 53.

